The Meteoritical Society

Meteoritics & Planetary Science 54, Nr 5, 1133–1152 (2019)
doi: 10.1111/maps.13272

Origin of the metamorphosed clasts in the CV3 carbonaceous chondrite breccias of Graves Nunataks 06101, Vigarano, Roberts Massif 04143, and Yamato-86009

Kaori JOGO[1*], Motoo ITO[2], Shigeru WAKITA[3], Sachio KOBAYASHI[2], and Jong Ik LEE[1]

[1]Division of Earth-System Sciences, Korea Polar Research Institute, 26 Songdomirae-ro, Yeonsu-gu, Incheon 21990, South Korea
[2]Kochi Institute for Core Sample Research, JAMSTEC B200 Monobe, Nankoku, Kochi 783-8502, Japan
[3]Center for Computational Astrophysics, National Astronomical Observatory of Japan, 2-21-1 Osawa, Mitaka, Tokyo 181-8588, Japan
[*]Corresponding author. E-mail: kaorijogo@kopri.re.kr

(Received 24 January 2018; revision accepted 02 February 2019)

Abstract–We observed metamorphosed clasts in the CV3 chondrite breccias Graves Nunataks 06101, Vigarano, Roberts Massif 04143, and Yamato-86009. These clasts are coarse-grained polymineralic rocks composed of Ca-bearing ferroan olivine ($Fa_{24–40}$, up to 0.6 wt% CaO), diopside ($Fs_{7–12}Wo_{44–50}$), plagioclase ($An_{52–75}$), Cr-spinel (Cr/[Cr + Al] = 0.4, Fe/[Fe + Mg] = 0.7), sulfide and rare grains of Fe-Ni metal, phosphate, and Ca-poor pyroxene ($Fs_{24}Wo_4$). Most clasts have triple junctions between silicate grains. The rare earth element (REE) abundances are high in diopside (REE ~3.80–13.83 × CI) and plagioclase (Eu ~12.31–14.67 × CI) but are low in olivine (REE ~0.01–1.44 × CI) and spinel (REE ~0.25–0.49 × CI). These REE abundances are different from those of metamorphosed chondrites, primitive achondrites, and achondrites, suggesting that the clasts are not fragments of these meteorites. Similar mineralogical characteristics of the clasts with those in the Mokoia and Yamato-86009 breccias (Jogo et al. 2012) suggest that the clasts observed in this study would also form inside the CV3 chondrite parent body. Thermal modeling suggests that in order to reach the metamorphosed temperatures of the clasts of >800 °C, the clast parent body should have accreted by ~2.5–2.6 Ma after CAIs formation. The consistency of the accretion age of the clast parent body and the CV3 chondrule formation age suggests that the clasts and CV3 chondrites could be originated from the same parent body with a peak temperature of 800–1100 °C. If the body has a peak temperature of >1100 °C, the accretion age of the body becomes older than the CV3 chondrule formation age and multiple CV3 parent bodies are likely.

INTRODUCTION

CV3 carbonaceous chondrites are an important group of primitive meteorites, which typically contain a diverse range of components of presolar grains, calcium-aluminum-rich inclusions (CAIs), chondrules, matrix fine grains, and dark inclusions, etc. (e.g., Brearley and Jones 1998). The study of those components in CV3 chondrites has provided fundamental insights into the evolution of the early solar system.

The CV3 chondrites are subdivided into the oxidized Allende-like ($CV3_{OxA}$), oxidized Bali-like ($CV3_{OxB}$), and reduced (CV_{Red}) subgroups based on the mineralogy, petrography, bulk chemistry, and oxygen isotopic compositions (McSween 1977; Weisberg et al. 1997). These subgroups experienced different types and degrees of aqueous/metasomatic alteration and thermal metamorphism (Krot et al. 1995, 1998a, 1998b, 2004). The $CV3_{OxB}$ chondrites experienced aqueous alteration that resulted in the formation of secondary fayalite, ferroan olivine, phyllosilicate, magnetite, Fe,Ni–sulfide, Fe,Ni–carbide, salite–hedenbergite pyroxenes, and andradite (Krot et al. 2004; MacPherson et al. 2017; Ganino and Libourel 2017). The $CV3_{OxA}$ chondrites experienced relatively high-temperature Fe-alkali-halogen metasomatic alteration (Brearley 1997, 1999; Bonal et al. 2006) that resulted in the formation of secondary ferroan olivine, nepheline, sodalite, andradite, grossular, wollastonite, kirschsteinite, and salite–hedenbergite pyroxenes (Kimura and Ikeda 1995; Ikeda and Kimura 1995; Krot et al. 1995, 1998a, 1998b, 2004; MacPherson et al. 2017; Ganino and Libourel 2017). The $CV3_{Red}$ chondrites experienced metasomatic alteration similar to that of the $CV3_{OxA}$ chondrites but to a smaller degree (Krot et al. 1995, 1998a, 1998b, 2004).

The mineralogical, geochemical, and oxygen isotopic evidence exhibited by the three CV3 subgroups can be explained by two distinct scenarios for the asteroidal sources of the CV3 chondrites (1) each CV3 subgroup might be derived from a distinct parent body or (2) all CV3 subgroups might have originated from a single heterogeneously altered parent body (e.g., Krot et al. 2000a; Greenwood et al. 2010). The latter scenario might be more consistent with the evidence that many CV3 brecciated chondrites show mixed lithologies of different CV3 subgroups (Krot et al. 2000a; Tomeoka and Tanimura 2000; Jogo et al. 2009), or the Ca-Fe-rich secondary minerals (e.g., kirschsteinite, andradite, Ca-rich pyroxene) in different CV3 subgroups could have formed at similar formation conditions (Ganino and Libourel 2017).

The CV3 chondrites also contain lithic clasts which might have originated from the CV3 chondrite parent body (e.g., dark inclusions and metamorphosed clasts). The dark inclusions commonly occur in Allende and, less commonly, in some other CV3 chondrites (e.g., Kojima and Tomeoka 1996). They consist of fine-grained matrix and/or chondrules and CAIs, and would have experienced extensive aqueous alteration and thermal metamorphism in the asteroidal settings (e.g., Kojima and Tomeoka 1996). They are similar in chemical and oxygen isotopic compositions and mineralogical characteristics to CV3 chondrites (Fruland et al. 1978; Bischoff et al. 1988; Johnson et al. 1990; Kojima and Tomeoka 1996), suggesting that the dark inclusions are fragments of the CV3 chondrite parent body (e.g., Kojima and Tomeoka 1996). In contrast, the metamorphosed clasts are also thought to form inside the CV3 chondrite parent body. They are olivine-rich aggregates that occur in Mokoia and Yamato (Y)-86009 (e.g., Cohen et al. 1983; Krot and Hutcheon 1997; Jogo et al. 2012). They typically show coarse-grained granoblastic textures with triple junctions and occasionally preserve chondrule-like textures. Jogo et al. (2012) inferred that the clasts experienced high-temperature metamorphism (>800 °C) in the interior of the CV3 parent body based on the similarities of oxygen isotope compositions, bulk chemical compositions, and mineralogical characteristics of the clasts and CV3 chondrites.

Other groups of meteorites may also have a link to CV3 chondrites. For example, metamorphosed CK chondrites and CV meta-chondrites (Northwest Africa 3133 and 1839) show similar mineralogy and chemical and isotopic compositions to the CV3 chondrites (e.g., Irving et al. 2004; Schoenbeck et al. 2006; Greenwood et al. 2010; Wasson et al. 2013; Chaumard et al. 2014; Chaumard and Devouard 2016). It is conceivable that such meteorites originated from the deep interior of the CV3 parent body. Moreover, magnetic studies of CV3 chondrites suggest that the parent body may have undergone melting, igneous differentiation, and Fe-Ni core formation (e.g., Carporzen et al. 2011; Elkins-Tanton et al. 2011; Fu and Elkins-Tanton 2014; Shah et al. 2017).

In this study, we found the metamorphosed clasts in four CV3 chondrite breccias: Graves Nunataks (GRA) 06101, Vigarano, Roberts Massif (RBT) 04143, and Y-86009. We described the mineralogical and petrological characteristics of the clasts and conducted ion microprobe analyses for REE abundances of the clasts in the Y-86009 breccia. A comparison between the formation conditions of the clasts and the thermal histories of the CV3-like body has enabled us to constrain the accretion time and thermal history of the parent body of the clasts.

METHODS

Mineralogy and Petrology

We have investigated twelve CV3 chondrites (LaPaz Icefield [LAP] 022066, LAP 04843, LAP 02228, MET 00430, MET 01074, Queen Alexandra Range [QUE] 97186, Thiel Mountains [TIL] 07007, Asuka [A]-881317, GRA 06101, Vigarano, RBT 04143, and Y-86009 chondrites) and found metamorphosed clasts in four CV3 chondrites (GRA 06101, Vigarano, RBT 04143, and Y-86009). The chemical compositions, and mineralogical and petrological characterization of metamorphosed clasts were obtained by scanning electron microscopy (SEM) and field-emission electron probe microanalyzer (FE-EPMA). A 25 nm thick carbon film was applied to the sample surfaces prior to the SEM and EPMA analyses in order to eliminate electrostatic charging. The SEM (JSM-6610 at Korea Polar Research Institute) was equipped with a backscattered electron (BSE) imaging system and an energy-dispersive X-ray spectrometer. X-ray spectra were obtained at a 15 keV accelerating voltage and a beam current mode of ss50 to identify the minerals. Chemical compositions of clasts were obtained using the FE-EPMA (JEOL JXA-8530F at Korea Polar Research

Institute) equipped with a wavelength dispersive X-ray spectrometer. Quantitative chemical analyses were operated at a 20 kV accelerating voltage and a 10 nA beam current. The ZAF correction method was applied.

REEs

REE measurements were performed on polished sections of standards (GM 1–5, NIST 612, and JGb1, details are described below) and the meteorite sample of Y-86009 by using an ion microprobe (AMETEK CAMECA ims-6f) at Kochi Institute for Core Sample Research, JAMSTEC. We used the technique of a voltage offset to the sample and an energy filtering of the secondary ions in order to eliminate interferences of complex molecules, hydrides, and monoxides from the secondary ion signals of the REEs (e.g., Fahey 1998). The detailed measurement conditions and techniques are described below.

We used a focused $^{16}O^-$ primary beam of ~10–30 μm in diameter with an intensity of ~3–14 nA. The beam intensity (size) was changed depending on sizes of target minerals. The negative primary ^{16}O ions were accelerated with 13 keV to sputter the sample surface. Positive secondary ions of masses 26 ($^{26}Mg^+$), 30 ($^{30}Si^+$), and 138–175 ($^{138}Ba^+$, $^{139}La^+$, $^{140}Ce^+$, $^{141}Pr^+$, $^{142}Nd^+$, $^{147}Sm^+$, $^{151}Eu^+$, $^{153}Eu^+$, $^{158}Gd^+$, $^{159}Tb^+$, $^{163}Dy^+$, $^{165}Ho^+$, $^{166}Er^+$, $^{169}Tm^+$, $^{172}Yb^+$, and $^{175}Lu^+$) were accelerated with −4.4 keV, and energy was filtered using a −60 V offset with a 30-eV energy window. A counting time for each secondary ion was 2–10 s. One analysis consisted of 20 cycles and the total acquisition time was ~1 h. Each run started after stabilization of the secondary ion beam intensity following pre-sputtering.

First, we measured three kinds of standards (GM 1–5, NIST 612, and JGb1) to determine REE-oxide/REE ratios and relative sensitivity factors (RSFs) for REE/Si and REE/Mg. Under energy filtering conditions, complex molecular ions are effectively eliminated and the principal remaining interferences for REE measurements are REE monoxides (e.g., Fahey 1998). Synthetic diopside glass standards with a stoichiometry of $CaMgSi_2O_6$ (GM 1–5, see details in Ito and Messenger 2016) were measured to determine REE-oxide/REE ratios. In each standard glass, the suite of elements was chosen to avoid isobaric interferences of REEs with other REEs or their oxide peaks. We verified that REE-oxide/REE ratios are sufficiently low as < 0.3 under energy filtering conditions of −60 V offset (Table S1 in supporting information). We totaled the counts for each of the isotopes over all of the cycles. Then, the REE abundances were corrected by the contributions of REE-oxide. The NIST 612 and JGb1 were used for the standards to obtain RSFs for REE/Si and REE/Mg, respectively. The true REE abundances were calculated by the equations $[REE]_{true} = RSF \times [REE^+/Si^+]_{SIMS} \times [Si]_{EPMA}$ or $[REE]_{true} = RSF \times [REE^+/Mg^+]_{SIMS} \times [Mg]_{EPMA}$ ($[REE^+/Si^+$ or $Mg^+]_{SIMS}$ is the measured counts of REE^+/Si^+ or Mg^+ by SIMS; $[Si$ or $Mg]_{EPMA}$ is the Si or Mg concentration in the SIMS analysis spot determined by EPMA). We verified that RSFs were not changed with primary beam current of ~1–12 nA. Then, we are able to increase or decrease primary beam current (beam size) depending on sizes of target minerals. Obtained RSFs for REE/Si and REE/Mg are summarized in Table S1.

In the next step, we measured REE abundances of CAI melilite in the Y-86009 meteorite sample and corrected them by REE-oxide/REE ratios and RSFs. We checked whether the calculated REE abundances of CAI melilite in Y-86009 were consistent with the literature data of CAI melilite in CV3 chondrites (e.g., Ito and Messenger 2016). Finally, we measured REE abundances of each mineral in the clasts 1–3 and 6 in Y-86009. For the measurements on olivine, diopside, and plagioclase, we used Si as a reference signal to calculate absolute concentrations of REEs. In contrast, for the measurement on spinel, we used Mg as a reference signal to calculate absolute concentrations of REEs because spinel does not contain Si. The REE patterns in this study are reported relative to the mean of CI chondrites from Anders and Grevesse (1989).

Thermal Modeling

Thermal modeling of the CV3-like body was performed. The framework of our model calculations is described in detail in Wakita and Sekiya (2011) and Jogo et al. (2017). We ran models for bodies with radii of 30, 50, 100, and 200 km (any given values between 10 km and 1,000 km for the planetesimals' radius; Johansen et al. 2007; Cuzzi et al. 2008; Chambers 2010) to reach peak temperatures of 800 and 1100 °C (minimum and maximum formation temperature of the metamorphosed clasts; see details in the Mineralogy and Petrology of the Metamorphosed Clasts in the GRA 06101, Vigarano, RBT 04143, and Y-86009 Breccias; Thermal Modeling of the CV3-Like Body; and Origin of the Metamorphosed Clasts in the GRA 06101, Vigarano, RBT 04143, and Y-86009 Breccias sections). We considered spherically symmetric, instantaneously accreting bodies. A heat-conduction equation was solved numerically using a finite difference method and an explicit method of integral evaluation (Wakita and Sekiya 2011). We assumed that ^{26}Al ($t_{1/2}$ = 0.72 Ma) was the only radiogenic heat source with the initial $^{26}Al/^{27}Al$ ratio of 5.25×10^{-5} that was uniformly distributed in the protoplanetary disk by the time the majority of CAIs formed (MacPherson et al. 1995; Connelly et al. 2012; Kita et al. 2012).

Several studies consider both ^{26}Al and ^{60}Fe as heat sources for the parent bodies of meteorites. However, the initial ^{60}Fe/^{56}Fe ratio in the solar system is still uncertain, and the estimated values are different in the literature (the initial ^{60}Fe/^{56}Fe ratio of $<1 \times 10^{-8}$ to $\sim 2 \times 10^{-7}$; Spivak-Brindorf et al. 2011; Tang and Dauphas 2011; Telus et al. 2011). In addition, recently, Telus et al. (2016) reported that there was significant exchange of Fe and Ni between chondrules and the matrices during low-temperature alteration in the unequilibrated ordinary chondrites and that the Fe-Ni system was not closed. Because the estimated temperature profile of planetesimals by thermal modeling does not change when the initial ^{60}Fe/^{56}Fe ratios are 1.0×10^{-8} and 2.0×10^{-7} (any given values between the literature data of initial ^{60}Fe/^{56}Fe ratios of $<1 \times 10^{-8}$ to $\sim 2 \times 10^{-7}$; Wakita and Sekiya 2011), we did not add ^{60}Fe as an additional heat source for the parent body in this paper. We assumed no fluid-flow in the model, because there is no evidence that fluid-driven redistribution exceeds the ~cm scale based on chemical data on carbonaceous chondrites (e.g., Keller et al. 1994; Krot et al. 1998a, 1998b; Bland et al. 2009; Stracke et al. 2012; MacPherson and Krot 2014) and the low permeability of initial chondritic materials (Bland et al. 2009).

We assumed that hydration and oxidation reactions occurred at 0 °C, soon after the melting of ice. We assumed that the initial (unaltered) rocks in the CV3 parent body contained elements with the atomic ratio Si:Fe:Mg = 1:1:1, which is consistent with the approximate ratios of the solar abundance (Lodders 2003) and close to bulk chemical compositions of CV3 chondrites; the original mineralogy was assumed to be olivine, $(Mg_{0.5}Fe_{0.5})_2SiO_4$ (Hutchison 2007; Wakita and Sekiya 2011). The simplified hydration-oxidation reaction of $(Mg_{0.5}Fe_{0.5})_2SiO_4$ [olivine] + H_2O [aq] = 1/3 $(Mg_{0.8}Fe_{0.2})_3Si_2O_5(OH)_4$ [serpentine] + 1/12 $(Mg_{0.8}Fe_{0.2})_3Si_4O_{10}(OH)_2$ [talc] + 1/4Fe_3O_4 [magnetite] + 1/4 H_2 is assumed.

Talc is a minor mineral in the CV3$_{OxA}$ Allende chondrite (Brearley 1997). Brearley (1997) proposed that talc is a metamorphic mineral produced during thermal metamorphism in the Allende parent body. Because of the similarities of oxygen isotopic compositions, bulk chemical compositions, and mineralogical characteristics of Allende and to a certain extent clasts, one of precursors of the clasts would experience similar alteration conditions as Allende (Jogo et al. 2012). This implies that the precursors of the clasts would also contain talc, and thus it would be plausible to form talc in the hydration–oxidation reaction.

The hydration–oxidation reaction was assumed to be an enthalpy of 2.77×10^5 kJ kg^{-1}, as calculated from enthalpies of compounds at 25 °C (Holland and Powell 1998). We assumed that the reaction enthalpy is the same at 0 and 25 °C. We also assumed the following initial constants for the CV3 parent body: temperature of −123 °C (corresponds to 3–4 AU in the protoplanetary disk), Al content of 1.75 wt% (bulk Al contents of CV3 chondrites; Hutchison 2007), water/rock mass ratio of 0.1 (fayalite formation conditions in CV3$_{OxB}$ Bali chondrites; Zolotov et al. 2006). Physical properties and other details of modeling are described in Wakita and Sekiya (2011).

RESULTS

Mineralogy and Petrology of the Metamorphosed Clasts in the GRA 06101, Vigarano, RBT 04143, and Y-86009 Breccias

Metamorphosed clasts were observed in four CV3 chondrite breccias (GRA 06101, Vigarano, RBT 04143, and Y-86009) among the 12 CV3 chondrites that we studied (Table 1). We observed three metamorphosed clasts in Vigarano, four clasts in RBT 04143, one clast in GRA 06101, and 13 clasts in Y-86009 in the sections studied (Table 2). The clasts are coarse-grained, granular, polymineralic rocks with sizes ranging from 10 to 100 μm (e.g., Fig. 1). The clasts are composed of Ca-bearing ferroan olivine ($Fa_{24–40}$, up to 0.6 wt% CaO), Ca-poor and rich pyroxene ($Fs_{24}Wo_4$ and $Fs_{7–12}Wo_{44–50}$), plagioclase ($An_{52–75}$), Cr-spinel (Cr/[Cr + Al] = 0.4, Fe/[Fe + Mg] = 0.7), pyrrhotite, pentlandite, Ca-phosphate, and Fe-Ni metal (Tables 2 and S2 in supporting information). Olivine, pyroxene, and plagioclase commonly form triple junctions (e.g., Fig. 1). Olivine has rather uniform fayalite contents within individual clasts (Figs. 2a and 2b). There are, however, Fa variations between the clasts. Pyroxenes show different chemical compositions between the clasts, but uniform compositions within individual clasts (Fig. 2c). Plagioclase is compositionally variable within individual clasts (Figs. 2d and 2e). These mineralogical and petrological characteristics of the metamorphosed clasts in the GRA 06101, Vigarano, RBT 04143, and Y-86009 breccias are similar to those in the Mokoia and Y-86009 breccias (Jogo et al. 2012).

Based on olivine-spinel (Fabries 1979) and high-Ca pyroxene thermometry (Kretz 1982), the estimated metamorphic temperatures recorded by the clasts range from approximately 700–800 °C. These temperatures are consistent with those recorded by the clasts in the Mokoia and Y-86009 breccias (Jogo et al. 2012). The high-Ca pyroxene equilibration temperature is estimated from equation 19b in Kretz (1982) using only the high-Ca pyroxene data.

Table 1. CV3 chondrites containing the metamorphosed clasts.

Subtype	Meteorite	Breccia/Nonbreccia	Clasts	Reference
OxA	GRA 06101	Breccia	Clasts	This study
	LAP 02206	Breccia	No clasts	This study
	LAP 04843	Breccia	No clasts	This study
	LAP 02228	Nonbreccia	No clasts	This study
OxB	Mokoia	Breccia	Clasts	[1] and [2]
	Y-86009	Breccia	Clasts	This study and [2]
	MET 00430	Nonbreccia	No clasts	This study
	MET 01074	Nonbreccia	No clasts	This study
	QUE 97186	Breccia	No clasts	This study
Red	Vigarano	Breccia	Clasts	This study
	RBT 04143	Breccia	Clasts	This study
	TIL 07007	Breccia	No clasts	This study
	A 881317	Breccia	No clasts	This study

[1] Cohen et al. 1983; [2] Jogo et al. 2012.

Table 2. Mineralogy of the metamorphosed clasts in the CV3 chondrite breccias.

			Mineralogy								
Sample	Section	Clast#	ol	Fa	px	Fs/Wo	pl	An	sp	sf	Others
Vigarano	Vigarano1	clast1	ol	29	px	24/4	pl	61			
	Vigarano2	clast1	ol	28–29			pl	57–63			
		clast2	ol	28–29			pl	66			
RBT 04143	RBT 04143-3	clast1	ol	35			pl	75	sp	sf	
		clast2	ol	24–25	px	n.m.	pl	n.m.			phs
		clast4	ol	31–33	px	12/44	pl	52–53	sp		
		clast5	ol	31							
GRA 06101	GRA06101	clast1	ol	36						sf	
Y-86009	Y-86009 UH1	clast4	ol	37			pl	62			
		clast5					pl	63	sp		
		clast6	ol	37	px	7-9/48–50			sp	sf	
		clast7	ol	37							
		clast8	ol	39–40	px	n.m.					
		clast9	ol	37							
		clast10	ol	37							
		clast11	ol	35–36					sp		
		clast12	ol	36							
		clast13	ol	38					sp		
		clast14	ol	36					sp		
		clast15	ol	40					sp		
		clast16	ol	38–40					sp		
Y-86009	Y-86009 UH1	clasts 1–3	ol	36–37	px	9/49	pl		sp	sf	met
Mokoia			ol		px		pl		sp	sf	met, nph, phs

n.m. = not measured due to small size; met = metal; nph = nepheline; ol = olivine; phs = phosphate; pl = plagioclase; px = pyroxene; sf = sulfide; sp = spinel; Data of the metamorphosed clasts in Mokoia and the clasts 1–3 in Y-86009 are referred from Jogo et al. (2012).

REE Abundances of the Metamorphosed Clasts in the Y-86009 Breccia

The clasts in Y-86009 show features that are typical of all the clasts. Next, we measured REE abundances of olivine, diopside, plagioclase, and spinel in clasts 1–3 and 6 in the Y-86009 chondrite (Figs. 1c–f). Mineralogy and oxygen isotopic compositions of clasts 1–3 have already been reported in Jogo et al. (2012). REE data of each SIMS measurement spot are shown in Table S3 in supporting information. Note that some of the analysis spots contain multiple REE-bearing phases and

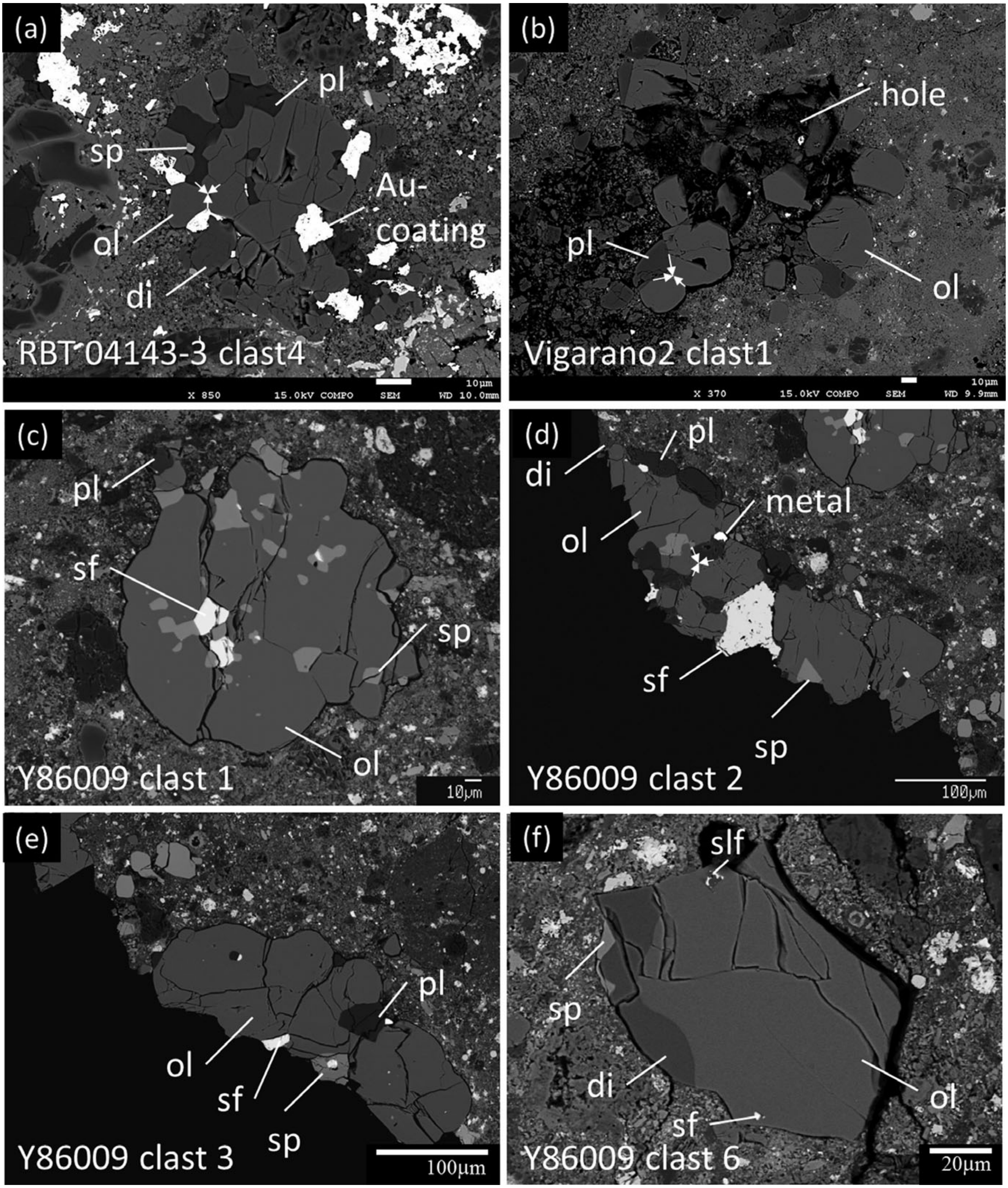

Fig. 1. Backscattered electron images of the metamorphosed clast 3 in RBT 04143-3 (a), the clast 1 in Vigarano2 (b), and the clasts 1–3 and 6 in Y-86009UH1 (c–f). The clasts are embedded in the matrix. Triple junctions are indicated by arrows. di = diopside; ol = olivine; pl = plagioclase; sp = spinel; sf = sulfide. The section of RBT 04143-3 contains Au-coating which was used for another study.

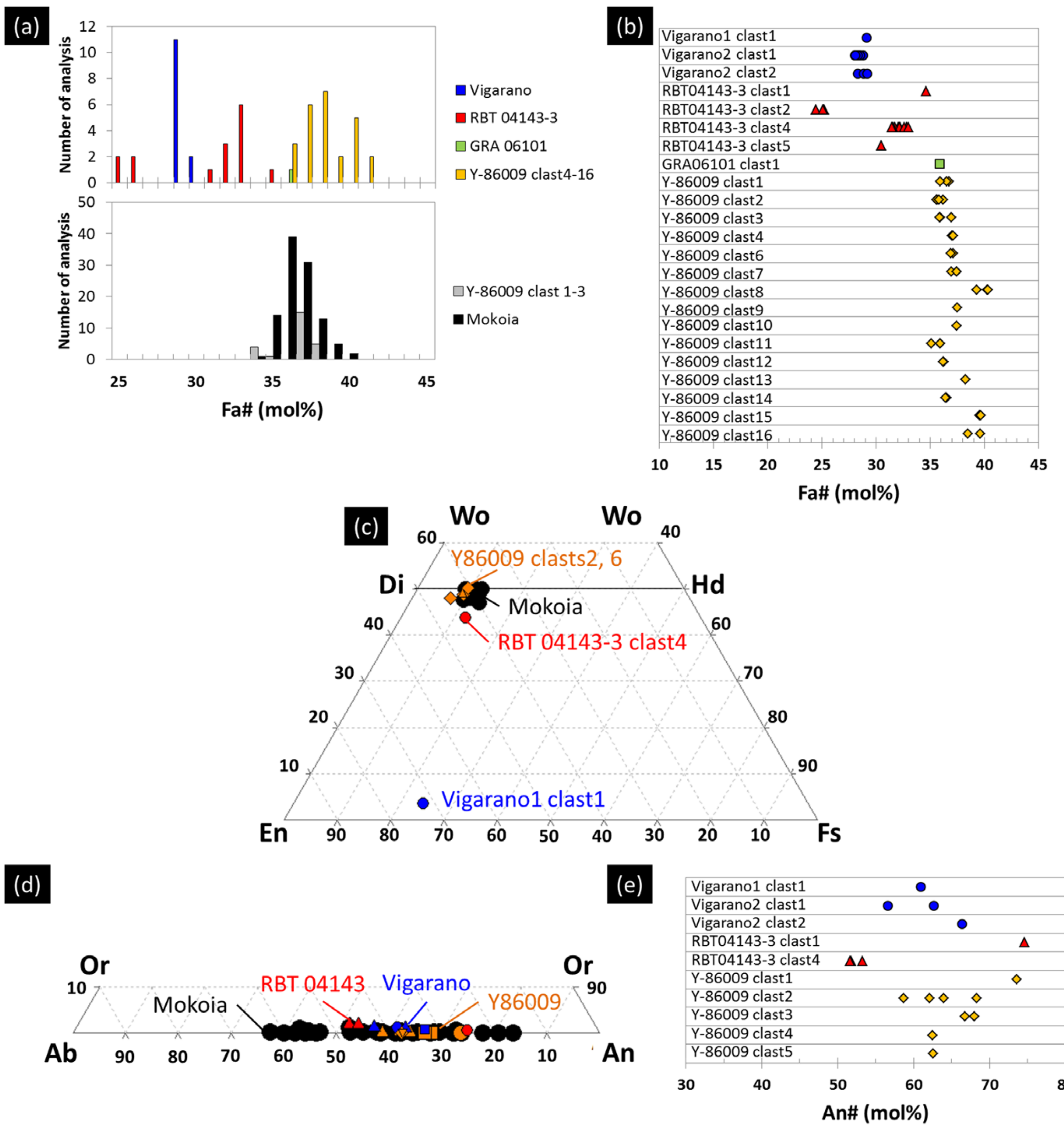

Fig. 2. Chemical compositions of olivine, pyroxene, and plagioclase in the metamorphosed clasts from the GRA 06101, Vigarano, RBT 04143, and Y-86009 breccias. a) Histogram of Fa contents (mol%) in olivine. b) Fayalite contents (Fa, mol%) in olivine. Fa contents are uniform within an individual clast but various between the clasts. c) Enstatite (En), ferrosilite (Fs), and wollastonite (Wo) contents (mol%) in pyroxenes. Compositions are various between the clasts. d) Albite (Ab) and anorthite (An) contents (mol%) in plagioclase. e) An content (mol%) in plagioclase. Compositions of the clasts in the Mokoia and Y-86009 breccias (Jogo et al. 2012) are shown for references. (Color figure can be viewed at wileyonlinelibrary.com.)

that corrections were required. For example, REE data for spinel in clast 1 (Y86UH1clast1_sp#1) are corrected for a contribution from olivine based on REE concentrations in olivine (averaged REE abundances of Y86UH1clast1_ol#1~3) and modal abundance of olivine in the SIMS measurement spot of Y86UH1clast1_sp#1. Corrected REE concentrations of minerals in each clast are shown in Table 3 and Fig. 3.

The olivine grains in all clasts 1–3 and 6 show similar fractionated REE patterns, which are enriched in HREEs compared to LREEs (La = ~0.01–0.08 × CI and Lu = ~1.04–1.44 × CI) (Fig. 3a). The LREE concentrations are slightly variable among olivine grains, whereas HREE concentrations are consistent within errors. The REE concentrations in plagioclase are similar in clasts 2 and 3 (Table 3). Plagioclase has fractionated REE patterns (Fig. 3b) with enriched LREE compared to HREE (La = ~3.36–3.79 × CI and Lu = ~0.04–0.20 × CI). It shows a positive Eu anomaly, with values up to several hundred ppb (Table 3), and shows a large positive Eu anomaly. REE concentrations in diopside were obtained from only two grains in clast 6 due to their small sizes and rare abundances. Both diopside grains have similar high REE concentrations with values up to several hundred to several thousand ppb (Table 3). These grains have slightly fractionated REE patterns (Fig. 3c) and are enriched in HREE compared to LREE (La = ~5.44–6.06 × CI and Lu = ~8.55–9.64 × CI). Small positive Eu anomalies were observed. Spinel has low REE concentrations with up to several hundred ppb and shows a flat REE pattern with large uncertainties (La = ~0.49 × CI and Lu = ~0.32 × CI) (Table 3; Fig. 3d). The REE concentrations of olivine in the clasts are similar to those in the CV3 Vigarano chondrules (e.g., Jacquet et al. 2012), but different from those in the CV3 matrix (e.g., Hua et al. 1996; Inoue et al. 2004; Bland et al. 2005; Martin et al. 2013; Jogo et al. 2018), CK5–6 and L6 chondrites (e.g., Curtis and Schmitt 1979; Martin et al. 2013), primitive achondrites (acapulcoites and lodranites; e.g., Floss 2000), and ureililites (e.g., Guan and Crozaz 2000) (Fig. 4). The REE concentrations of diopside and plagioclase are different from those in the CV3 Vigarano chondrule, CK5–6 and L6 chondrites, primitive achondrites, and ureilites (Fig. 4). We have measured REE abundances of olivine, diopside, and plagioclase with different grain sizes (20–80 μm in diameter) to verify diffusive disturbance on REE patterns and abundances during thermal alteration. We did not observe any correlation between REE abundances or patterns and grain sizes in each olivine grain in clast 1 (Figs. 5a and 5b). In clasts 2, 3, and 6, we cannot discuss such correlations because of the small numbers of REE data in each clast (Fig. 5).

Thermal Modeling of the CV3-Like Body

We numerically modeled the temperature profiles of the CV3-like body, using various sizes (30–200 km radius) and peak temperatures (800–100 °C). Thermal histories of the body with different sizes and peak temperatures are similar (Fig. 6). The decay of ^{26}Al gradually heated the body, reaching 0 °C and melting ice approximately 0.1–0.2 Ma after the initial accretion. The melting of ice led to rapid warming due to exothermic hydration of olivine to phyllosilicates such as serpentine. Aqueous alteration began almost simultaneously (within 0.1 Ma) throughout the body. After water was consumed, the decay of ^{26}Al continued to raise the internal temperature and thermal metamorphism occurred. When heat loss by radiation exceeded the decay heat of ^{26}Al, the temperature of the body started to decrease. Smaller sized bodies began cooling at earlier times.

The estimated accretion age is dependent on size and peak temperature of the body. The earlier accreted body can reach higher peak temperature than the later accreted body if they have same sizes. For example, in the case of the body with 30 km in radius, the body with accretion age of ~2.1 Ma after CAI formation could reach ~1100 °C (red solid line in Fig. 6). If the same-sized body accreted at ~2.5 Ma after CAI formation, it could only reach ~800 °C (red dashed line in Fig. 6).

In contrast, the larger sized body can reach higher peak temperature than the smaller sized body if they accreted at the same time. This is the reason why the accretion age of the body with 30 km in radius (red solid and dashed lines in Fig. 6) is 0.1 Ma earlier than those of the bodies with 50–200 km radius (green, black, purple solid and dashed lines in Fig. 6). The accretion ages of the bodies with 50–200 km in radius are almost the same (e.g., green, black, purple solid and dashed lines in Fig. 6). This means that cooling from the surface of the body does not significantly affect the temperature at the center of the larger bodies.

To be the parent body of the metamorphosed clasts, the temperature of the CV3-like body is required to reach ≥800 °C (lower limit of the metamorphic temperature of the clasts; see the Mineralogy and Petrology of the Metamorphosed Clasts in the GRA 06101, Vigarano, RBT 04143, and Y-86009 Breccias section). This condition is fulfilled when the CV3-like body accreted at 2.5–2.6 Ma after CAI formation (dashed lines in Fig. 6). In contrast, the clast parent body should not exceed ~1100 °C, which is the melting point of silicates in CV3 chondrites (~1150 °C; Jurewicz et al. 1993); because plagioclase in the clasts does not occur interstitially to olivine or diopside but forms separate crystals (e.g., Fig. 1b), silicates in the clasts would not have been melted and thus the clasts would not have been heated at higher temperatures than the melting point of CV3 chondrites. This condition is fulfilled when the CV3-like body accreted at 2.1–2.2 Ma

Table 3. REE concentrations (ppb) in various phases of metamorphosed clasts 1, 2, 3, and 6 in the Y-86009 chondrite. REE data of Y86UH1clast1_sp1, Y86UH1clast2_pl1 and 2, Y86UH1clast3_pl1, and Y86UH1clast1_px2 are corrected for a contribution from olivine.

clast	clast1								clast2							
spot#	Y86UH1clast1_ol#1		Y86UH1clast1_ol#2		Y86UH1clast1_ol#3		Y86UH1clast1_sp1*calc		Y86UH1clast2_ol#1		Y86UH1clast2_ol#2		Y86UH1clast2_pl1*calc		Y86UH1clast2_pl2*calc	
Phase	Olivine		Olivine		Olivine		Spinel		Olivine		Olivine		Plagioclase		Plagioclase	
	Mean	1σ	Mean	1σ	Mean	1σ	Mean	1σ	Mean	1σ	Mean	1σ	Mean	1σ	Mean	1σ
La	4	5	18	7	11	6	116	40	4	3	4	3	5	4	851	44
Ce	12	9	29	10	23	9	233	61	4	3	4	3	4	4	929	51
Pr	1	2	4	3	3	3	16	15	1	1	1	1	<d.l.	–	60	12
Nd	7	13	11	13	6	9	112	91	1	4	1	4	<d.l.	–	174	48
Sm	3	10	6	10	<d.l.	–	33	53	<d.l.	–	<d.l.	–	<d.l.	–	<d.l.	-
Eu	5	17	2	8	<d.l.	–	<d.l.	–	0	7	0	7	5	11	822	231
Gd	15	23	9	16	8	14	61	87	3	7	3	7	4	10	32	33
Tb	2	3	3	3	4	3	7	13	1	1	1	1	2	2	3	5
Dy	37	29	38	23	32	20	91	78	6	8	6	8	20	17	43	21
Ho	10	8	20	8	18	8	26	23	10	5	10	5	13	7	22	8
Er	55	38	96	38	99	38	81	92	86	32	86	32	82	38	<d.l.	-
Tm	23	12	29	10	23	9	16	23	28	9	28	9	24	10	3	12
Yb	143	57	260	59	173	47	64	114	207	46	207	46	207	56	16	18
Lu	35	18	43	15	25	11	8	28	30	11	30	11	34	14	2	4

clast	clast3				clast6					
spot#	Y86UH1clast3_ol#1		Y86UH1clast3_pl3*calc		Y86UH1clast6_ol#1		Y86UH1clast6_px#1		Y86UH1clast6_px2*calc	
Phase	Olivine		Plagioclase		Olivine		Diopside		Diopside	
	Mean	1σ	Mean	1σ	Mean	1σ	Mean	1σ	Mean	1σ
La	1	2	888	44	2	2	1278	64	1422	142
Ce	6	5	982	51	7	4	3643	119	3785	252
Pr	1	2	72	12	1	1	570	42	575	88
Nd	3	7	208	52	4	7	2494	209	2374	426
Sm	4	8	14	13	1	4	780	120	617	223
Eu	2	7	798	231	<d.l.	–	464	143	575	179
Gd	<d.l.	–	31	34	0	5	1065	186	747	359
Tb	1	1	1	4	<d.l.	–	289	35	300	74
Dy	11	12	29	18	10	10	2883	205	3161	448
Ho	7	4	20	7	6	4	675	50	743	111
Er	64	30	10	48	45	22	2070	186	2245	417
Tm	26	9	7	13	18	7	328	37	340	84
Yb	207	49	<d.l.	–	177	40	1759	169	2247	427
Lu	31	12	1	5	26	10	208	40	234	98

<d.l. = below detection limit.

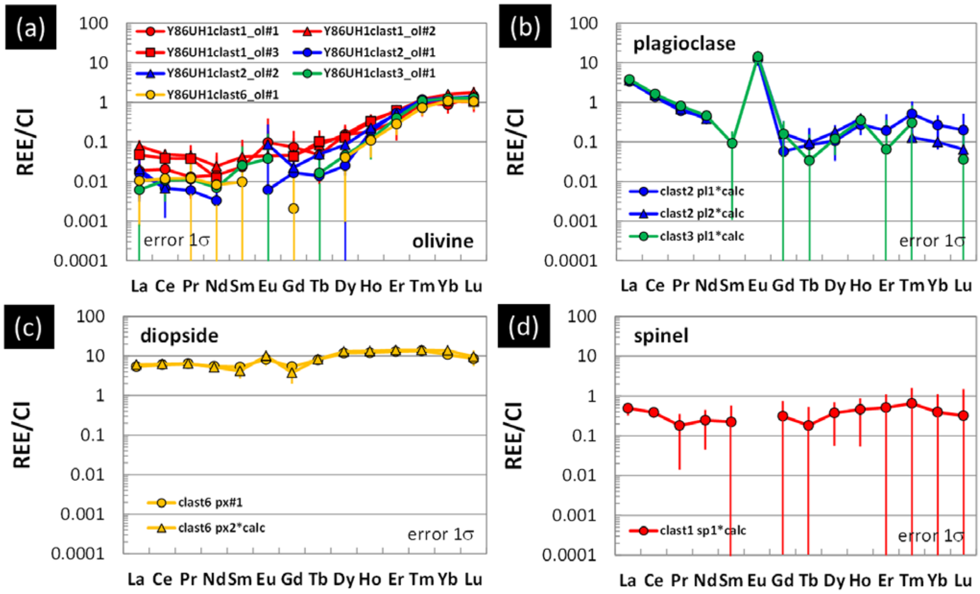

Fig. 3. CI-normalized rare earth element (REE) abundance patterns of olivine (a), plagioclase (b), diopside (c), and spinel (d) in the clasts 1–3 and 6 in the Y-86009 chondrite. REE data were obtained from the clasts 1–3 and 6 for olivine, the clasts 2 and 3 for plagioclase, the clast 6 for diopside, and the clast 1 for spinel. Error bars are 1σ. (Color figure can be viewed at wileyonlinelibrary.com.)

after CAI formation (solid lines in Fig. 6). Thus, the body with accretion ages of approximately 2.5–2.6 Ma to 2.1–2.2 Ma after CAI formation would be candidates for the parent body of the clasts.

Those estimated accretion ages of the bodies do not change significantly (0.1 Myr at most), if the modeling parameters (e.g., initial temperature, density, thermal conductivity) changed from our current values. For example, if the initial temperature changes to become lower (e.g., from −123 °C to −223 °C) or higher (e.g., 23 °C), the accretion age changes only approximately 0.1 Myr. The variation in other parameters such as density and thermal conductivity does not also make a big difference in our results and thus the errors on the estimated accretion age of the body would be ~0.1 Myr.

Figure 7 shows the temperature profile for the CV3-like bodies with radii of 100 km that accreted at 2.6 and 2.2 Ma after CV3 CAI formation (peak temperature of 800 and 1100 °C, respectively). These settings fulfilled the conditions of the clast parent body. In the body with a peak temperature of 800 °C, the metamorphosed clasts form within the inner region of the body (e.g., 0–65 km distance from the center of the body, Fig. 7a). In contrast, in the body with a peak temperature of 1100 °C, the clasts form at the edge of the inner area of the body where metamorphic temperature is in the range of 800–1100 °C (e.g., 0–90 km distance from the center of the body, Fig. 7b).

DISCUSSION

Origin of the Metamorphosed Clasts in the GRA 06101, Vigarano, RBT 04143, and Y-86009 Breccias

The metamorphosed clasts in the GRA 06101, Vigarano, RBT 04143, and Y-86009 breccias show coarse-grained granoblastic textures with triple junctions (Fig. 1), suggesting that they experienced sintering and high-temperature annealing of precursor materials. These clasts have similar mineralogical and petrological characteristics (Table 2; Figs. 1 and 2) with those in the Mokoia and Y-86009 breccias (Jogo et al. 2012). This suggests that the metamorphosed clasts found in this and previous studies would have a similar origin.

The clasts in the Mokoia and Y-86009 chondrites (Jogo et al. 2012) have oxygen isotope compositions that are close to the CCAM line and overlap with those of CV3 chondrites. It is an important line of evidence linking the clasts to the CV3 chondrite parent body. However, the CV3 chondrites are not the only group that plots on or close to the CCAM line; the CO and CK chondrites and to a certain extent ureilites have compositions on or close to the CCAM line (e.g., Clayton et al. 1976; Clayton and Mayeda 1999). This may suggest that the clasts have a genetic link to these meteorite groups. However, we found that REE concentrations of the clasts in the Y-86009 breccia are different from those in CK chondrites and ureilites

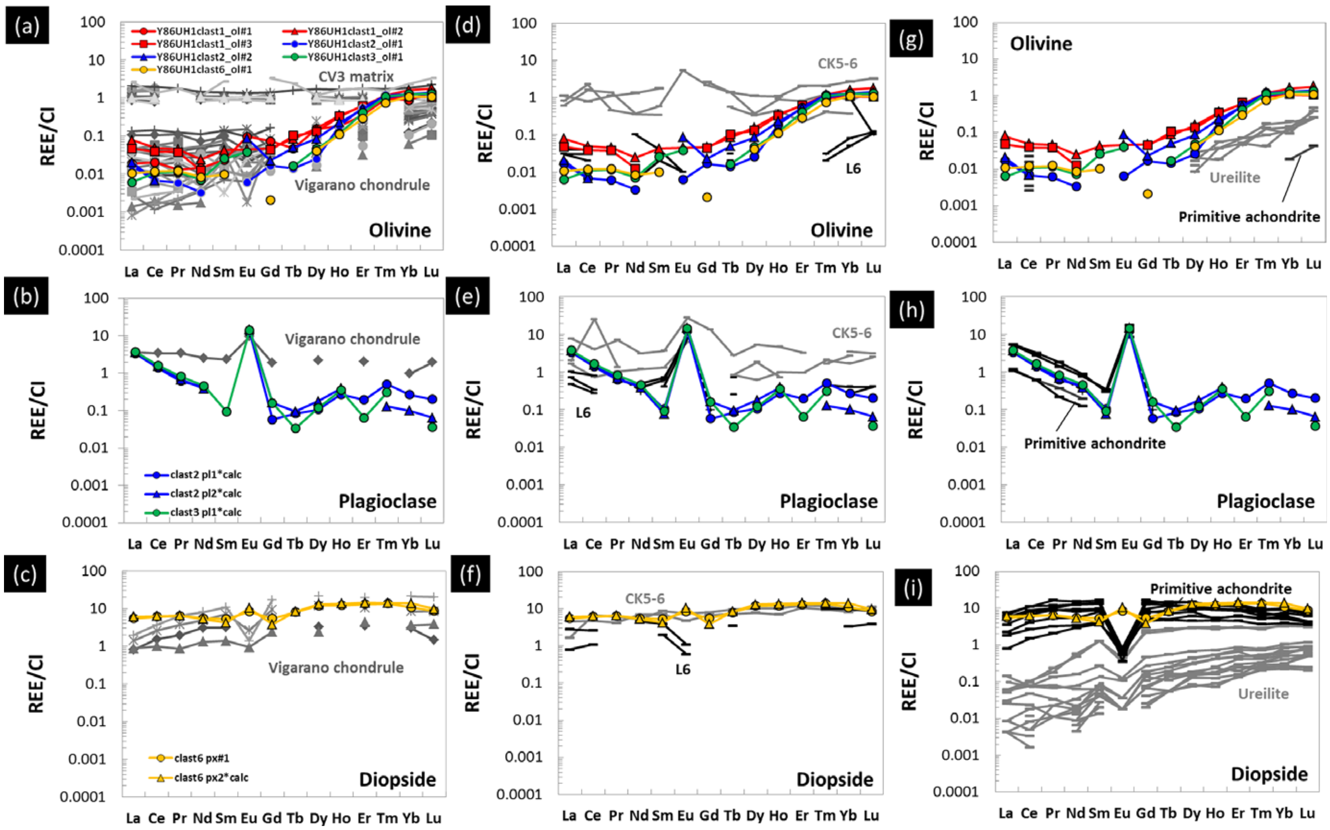

Fig. 4. CI-normalized REE abundances of olivine, plagioclase, and diopside in the clasts 1–3 and 6 in the Y-86009 chondrite and in CV3 chondrules and matrix (a, b, and c), metamorphosed CK5–6 and L6 chondrites (d, e, and f), primitive achondrites (acapulcoites and lodranites), and urelites (g, h and i). Data source: matrix in CV3 chondrites: Hua et al. (1996); Inoue et al. (2004); Bland et al. (2005); Martin et al. (2013); Jogo et al. (2018); chondrules in the CV3 Vigarano chondrite: Jacquet et al. (2012); CK5–6 chondrites: Martin et al. (2013); L6 chondrites: Curtis and Schmitt (1979); and primitive achondrites: Floss (2000); ureilites: Guan and Crozaz (2000). (Color figure can be viewed at wileyonlinelibrary.com.)

(Figs. 4d–i). In addition, the sizes of the chondrule-like materials preserved in the clasts are larger than those of chondrules in CO chondrites (Jogo et al. 2012). These evidences would support the idea that the precursor of the clasts would have been CV3 chondrite-like material (Jogo et al. 2012), not CO and CK chondrites and ureilites.

The precursor material of the clasts would have experienced various degrees of hydrothermal alteration prior to the thermal metamorphism in the CV3 chondrite parent body (Jogo et al. 2012). Olivine grains in one of the clasts in Mokoia (M25#4 in Jogo et al. 2012) have highly fractionated oxygen isotope compositions which are displaced from the CCAM line to the right by approximately 10‰ on a three-isotope oxygen diagram. They plot along the Allende mass-fractionation line defined by the whole-rock oxygen isotope compositions of the metasomatically altered chondrules from Allende (Jabeen et al. 1998, 1999; Ash et al. 1999; Young et al. 1999). Along this line, the oxygen isotope compositions of secondary minerals in CV3 chondrites that resulted from metasomatic alteration show a spread in $\delta^{18}O$ values up to 20‰ (Choi et al. 2000; Hua et al. 2005; Krot et al. 2006; Cosarinsky et al. 2008; Wasserburg et al. 2011). This suggests that the oxygen isotope compositions of the M25#4 olivines recorded the metasomatic alteration prior to the thermal metamorphism. Jogo et al. (2012) suggested that the precursor of the clasts experienced various degrees of hydrothermal alteration prior to thermal metamorphism. The similar process has been inferred for the $CV3_{OxA}$ chondrites and dark inclusions (e.g., Kojima and Tomeoka 1996; Krot et al. 1995, 1998a, 1998b, 2000b). The consistency of the oxygen isotopic compositions of the M25#4 clast and dark inclusions suggests that dark inclusions might be a precursor of the clast M25#4.

The clasts in the GRA 06101, Vigarano, RBT 04143, Y-86009, and Mokoia breccias would have been annealed at ~800–1100 °C within the CV3 parent body.

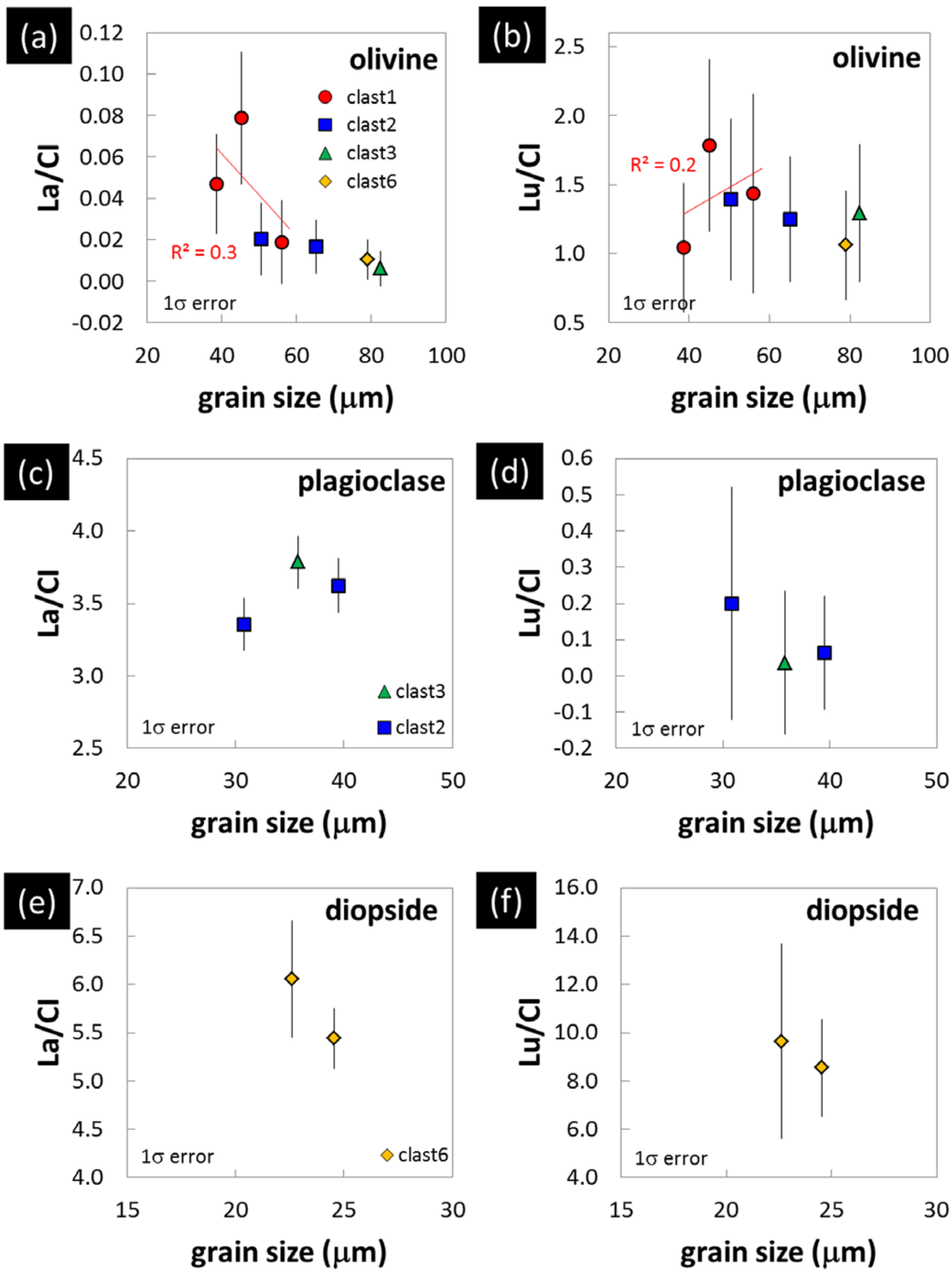

Fig. 5. Plot of CI-normalized La and Lu concentrations in olivine (a,b), plagioclase (c and d), and diopside (e and f) as a function of grain size in the clasts 1 (red), 2 (blue), 3 (green), and 6 (yellow) in the Y-86009 chondrite. Error bars for REE concentrations are 1σ. Correlation coefficients (R^2) for the mean values of La/CI or Lu/CI vs grain sizes are shown in (a and b). (Color figure can be viewed at wileyonlinelibrary.com.)

The minimum metamorphic temperature of ~800 °C is estimated from olivine-spinel and high-Ca pyroxene geothermometers (see the Mineralogy and Petrology of the Metamorphosed Clasts in the GRA 06101, Vigarano, RBT 04143, and Y-86009 Breccias section). In contrast, the maximum temperature of ~1100 °C is estimated from the melting point of CV3 chondrites (see the Mineralogy and Petrology of the Metamorphosed Clasts in the GRA 06101, Vigarano, RBT 04143, and Y-86009 Breccias and Thermal Modeling of the CV3-Like Body sections). Within this temperature range, each clast would have experienced different degrees of thermal metamorphism during their formation. The details are described below.

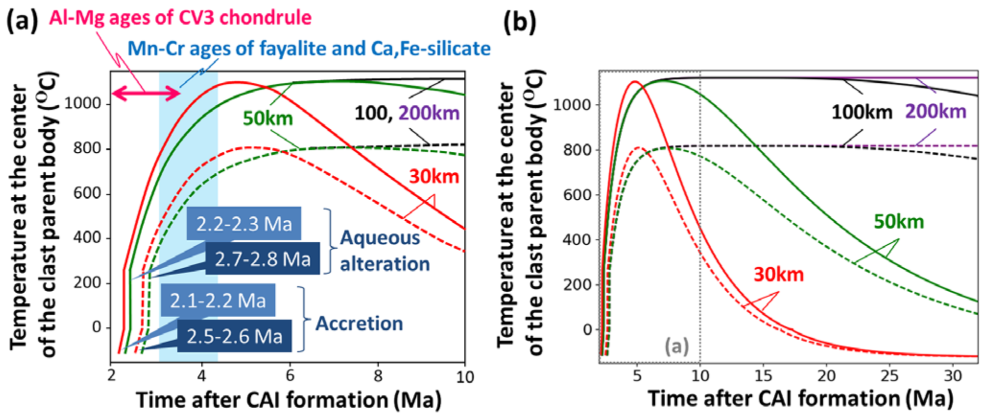

Fig. 6. Temperature evolution at the center of the parent body of the metamorphosed clasts with radii of 30 km (red), 50 km (green), 100 km (green), and 200 km (purple). (a) is part of (b). The body would have accreted at 2.5–2.6 and 2.1–2.2 Ma after CAI formation in order to reach the peak temperature of 800 and 1100 °C, respectively. The pathways of temperature evolution of the body with 100 km and 200 km in radii are the same in the time range of this figure. Aqueous alteration with increasing temperature occurs at approximately ~2.7–2.8 and 2.2–2.3 Ma after CAI formation in the body with peak temperature of 800 and 1100 °C, respectively. Thermal metamorphism occurred after aqueous alteration. Al-Mg formation ages of CV3 chondrules (~2.0–3.4 Ma after CAI formation; Mishra and Chaussidon 2014; Nagashima et al. 2017) and Mn-Cr ages of fayalite and Ca,Fe-silicates (~3.2–4.2 Ma after CAI formation; Doyle et al. 2015; Jogo et al. 2017; MacPherson et al. 2017) are also shown. (Color figure can be viewed at wileyonlinelibrary.com.)

The clasts can be classified into two types based on the homogeneity of Fa content in olivine and An content in plagioclase within individual clasts: [type 1] the clasts with homogeneous olivine and plagioclase compositions (e.g., the RBT 04143 clast 4 and the Y-86009 clast 3, Fig. 2) and [type 2] the clasts with homogeneous olivine compositions but heterogeneous plagioclase compositions (e.g., the Vigarano 2 clast 1 and the Y-86009 clast 2, Fig. 2). Similar chemical homogeneous/heterogeneous compositions of olivine and plagioclase were found in the metamorphosed clasts in the Mokoia and Y-86009 breccias (Jogo et al. 2012). The observed olivine and plagioclase compositions in the clasts would have resulted from diffusive exchanges of Fe-Mg in olivine and CaAl-NaSi in plagioclase during thermal metamorphism in the CV3 chondrite parent body (Jogo et al. 2012). Slower diffusion rates of CaAl-NaSi in plagioclase than those of Fe-Mg in olivine under fO_2 of CV3 chondrites (Fig. S1 in supporting information) (Grove et al. 1984; Dohmen and Chakraborty 2007; Righter and Neff 2007) suggest that the type 1 clasts with homogeneous olivine and plagioclase compositions experienced stronger degrees of thermal metamorphism (i.e., higher temperature and/or longer duration) than the type 2 clasts with homogeneous olivine and heterogeneous plagioclase compositions.

It remains unclear whether the REE compositions of each of the minerals in the clasts reflect their precursor compositions (i.e., CV3 chondrites) or were homogenized during thermal metamorphism. Olivine grains in the Y-86009 clast 1 show no correlation between grain sizes and REE concentrations (Fig. 5a), suggesting that REE diffusion did not occur or would have been completed during thermal metamorphism. Both possibilities are supported by the similar REE compositions of the Y-86009 clast 1 olivine with those of CV3 chondrules (Fig. 4a) and the time scale of thermal metamorphism estimated from the thermal modeling of CV3-like body (see details in the Thermal History of the Clast Parent Body section). In other clasts, we cannot discuss whether olivine, plagioclase, and diopside preserve the LREE compositions of precursors or are modified during thermal metamorphism because of the small numbers of REE data in each clast (Fig. 5). Further studies are needed.

Thermal History of the Clast Parent Body

We calculated the thermal histories of the clasts parent body as defined by the CV3 chondritic conditions (e.g., bulk Al contents and water/rock ratio) with radius of 30–200 km. To reach ~800–1100 °C (minimum and maximum metamorphic temperature of the clasts) at the center of the body, the body should accrete from ~2.5–2.6 Myr to ~2.1–2.2 Myr after CAI formation (Fig. 6). In such a body, the metamorphosed clasts formed in the inner area where metamorphic temperature is 800–1100 °C (e.g., 0–90 km distance from the center of the body with peak temperature of 1100 °C and radius of 100 km, Fig. 7b). In the same body, CV3 chondrites formed in the outer area and the “less-metamorphosed

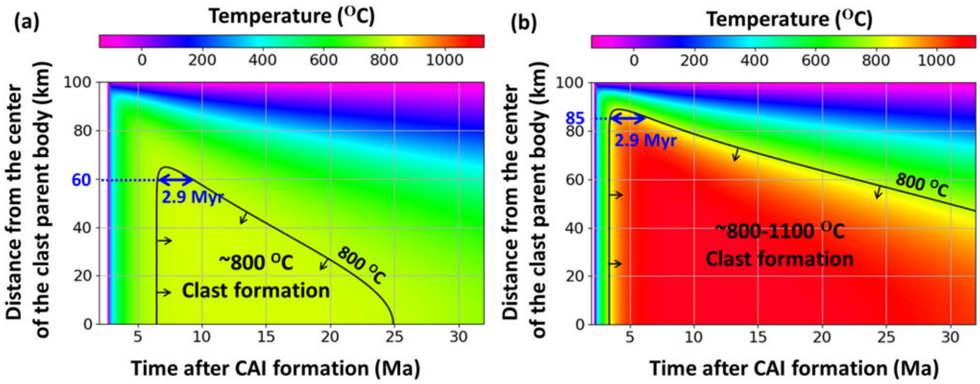

Fig. 7. Temperature profile of the 100 km radius body with the accretion age of ~2.6 Ma after CV3 CAIs and peak temperature of ~800 °C (a) and with the accretion age of ~2.2 Ma after CV3 CAIs and peak temperature of ~1100 °C (b). Temperature differences are indicated by the color scale. Solid lines are isothermal lines of 800 °C. The metamorphosed clasts formed at inner areas of the body where the temperature of 800–1100 °C is shown by arrows. Thermal metamorphism at ~800 °C continued shorter than ~2.9 Myr at > 60 and > 85 km distance from the center of the body with peak temperature of 800 and 1100 °C, respectively. (Color figure can be viewed at wileyonlinelibrary.com.)

Table 4. Time required to complete LREE exchange in a 50 μm sized olivine grain. The holding time at ~800–1100 °C at the center of the clast parent body inferred from thermal modeling is also shown.

T (°C)	LREE diffusion time (Myr)	Peak T of the body (°C)	The holding time at ~800–1100 °C at the center of the body (Myr)			
			R = 30 km	R = 50 km	R = 100 km	R = 200 km
800	2.9	800	1.0	2.6	19.2	>25.7
800	2.9	1100	4.5	11.3	>28.5	>28.5
900	0.2	1100	3.6	9.2	>28.1	>28.1
1000	15.6	1100	2.4	6.7	>27.5	>27.5
1100	0.9	1100	0.5	1.9	18.1	>25.8

T = temperature; R = radius of the body.

clasts" which preserve chondrule-like textures (Jogo et al. 2012) formed in the intermediate layers. If the peak temperature of the body was >1100 °C, the clasts would form at the intermediate layers of the body where the metamorphic temperature is 800–1100 °C.

The size of the parent body in which the Y-86009 clast 1 formed can be constrained by comparing the LREE diffusion time scale and the duration of the thermal metamorphism inferred from thermal modeling. As discussed in the Origin of the Metamorphosed Clasts in the GRA 06101, Vigarano, RBT 04143, and Y-86009 Breccias section, the LREE abundances of the Y-86009 clast 1 olivine grains could reflect their precursors or might be homogenized during thermal metamorphism. Based on diffusion coefficients for LREEs in olivine, thermal metamorphism at 800–1100 °C for ~0.2–20 Myr is required to complete LREE exchange in a 50 μm sized olivine grain under fO_2 of CV3 chondrites (Table 4; Fig. S1) (Righter and Neff 2007; Cherniak 2010). Comparing this duration with thermal modeling, we found that the Y-86009 clast 1 could form in a relatively small body (e.g., 30 and 50 km radius body with a peak temperature of 800 °C), or the outer region of a large body (e.g., ~60–100 km depth from the center of the 100 km radius body with peak temperature of 800 °C) if they preserve LREE abundances of their precursors (Table 5). The details are described below.

For example, at ~800 °C, the duration of thermal metamorphism should not be continued for longer than 2.9 Myr in order not to complete LREE exchange in a 50 μm sized olivine grain (Table 4). In the body with a peak temperature of 800 °C and radius of 30 and 50 km, the holding time at ~800 °C is longest at the center of the body and that is only ~1.0–2.6 Myr (Table 4). Because this duration is shorter than 2.9 Myr, LREE diffusion in olivine would not have been completed and the Y-86009 clast 1, which preserves the LREE abundances of its precursors, could have formed throughout the whole depth of such a small body (Table 5). In contrast, in a large body with a peak temperature of 800 °C and radius of 100 and 200 km, the Y-86009 clast 1, preserving the LREE

Table 5. Formation depth of the Y-86009 clast 1. The depth is shown as a distance from the center of the body.

Peak T of the body ( )	Radius of the body (km)	Clast formation T ( )	Clast formation depth (km)	
			Ol $\mathrm{LREE}_{\mathrm{precursor}}$	Ol $\mathrm{LREE}_{\mathrm{disturbed}}$
800	30	800	0–30	n.f.
	50	800	0–50	n.f.
	100	800	60–100	0–60
1100	100	800	85–100	0–85
		900	90–100	0–90
		1000	50–100	0–50
		1100	75–100	0–75

T = temperature; Ol $\mathrm{LREE}_{\mathrm{precursor}}$ and Ol $\mathrm{LREE}_{\mathrm{disturbed}}$ = the LREE abundances of the clast olivine reflect those of precursors or were disturbed during thermal metamorphism, respectively; n.f. = the clast did not form.

abundances of its precursors, could have formed only in the outer regions of the body where the holding time at 800 °C is shorter than 2.9 Myr (e.g., ~60–100 km depth from the center of the 100 km radius body, Table 5; Fig. 7a).

In contrast, relatively large bodies would be needed if the LREE abundances of the Y-86009 clast 1 olivine grains were homogenized during thermal metamorphism (Table 5). For example, at ~800 °C, the duration of thermal metamorphism needs to be continued for longer than 2.9 Myr in order to complete LREE homogenization in a 50 μm sized olivine grain (Table 4). In the inner area of the large body with the peak temperature of 800 °C and radius of 100 and 200 km, the holding time at ~800 °C is longer than 2.9 Myr (e.g., ~0–60 km depth from the center of the 100 km radius body, Fig. 7a), and thus the Y-86009 clast 1 having disturbed LREE abundances of olivine could have formed at the inner area of such a large body. In Table 5, we summarize the parent body size and burial depth where the Y-86009 clast 1 could have formed.

Implications for the Evolution Process of the Clast Parent Body

Since the clasts were observed only in the CV3 chondrite breccias (Table 1), the clasts would have been incorporated into the present structures of CV3 chondrites at a late stage of parent body evolution and not at the time of the initial accretion of the CV3 chondrite parent body. Some mechanism involved in moving these clasts from interior of the CV3 chondrite parent body and incorporating them within breccias are needed.

As such a mechanism, the impact gardening model has been proposed (e.g., Kracher et al. 1985). In this model, the breccias ought to be a chaotic mixture of CV3 chondrites, less-metamorphosed clasts, and metamorphosed clasts. However, the abundances of the less-metamorphosed clasts and metamorphosed clasts in the CV3 chondrites are low (e.g., <10 area%). It is difficult to explain such low abundance of the clasts by the impact gardening model. In order to resolve this problem, the clast parent body needs to be small and have low peak temperature (e.g., <100 km in radius and peak temperature of 800 °C), because the area where the clasts form becomes small in the smaller sized body with lower peak temperature. For example, the clast forms at ~80–90 area% of the 100 km radius body with peak temperature of ~1100 °C (Fig. 7b). If the same-sized body has the peak temperature of ~800 °C, the clast forms at ~60 area% of the body (Fig. 7b). Because 800 °C is the minimum formation temperature of the clasts, radius of the clast parent body is thought to be smaller than 100 km.

However, radius of >110–150 km is required to avoid disruption of the CV3 chondrite parent body by fluid pressure (Jogo et al. 2017). Wilson et al. (1999) suggested that parent bodies of carbonaceous chondrites would have been disrupted if fluid pressure produced during aqueous alteration exceeded the sum of lithostatic pressure and tensile strength of rocks. The fluid pressure in the CV3 chondrite parent body could be assumed to be ≥300 bars based on the necessary fluid pressure condition for the fayalite formation (fayalite is an alteration mineral produced during aqueous alteration in the CV3 chondrite parent body; Krot et al. 1995, 1998a, 1998b, 2004). By resolving an equation [fluid pressure] ≤ [lithostatic pressure] + [tensile strength of rocks] with the fluid pressure of ≥ 300 bars and tensile strength of rocks of ~100 bar (Rubin 1993), Jogo et al. (2017) found that a lithostatic pressure of ≥200 bars is required to avoid disruption of the CV3 chondrite parent body. In order to produce such lithostatic pressure, radius of >110–150 km is needed if we assumed a bulk density of the CV3 chondrite parent body as 2920–3500 kg m^{-3}, densities of CV, CO, CK, and CR carbonaceous chondrites (Consolmagno et al. 2008) and 2700 kg m^{-3}, a density of a mixture material of water and rock with water/rock mass ratio of 0.1 (water/rock = 0.1 is necessary for the fayalite formation in the $\mathrm{CV3}_{\mathrm{OxB}}$ Bali chondrite; Zolotov et al. 2006; Jogo et al. 2017).

The inconsistency between the estimated radius of the clast parent body by modal abundance of the clasts in the CV3 breccias and those by fluid pressure in the CV3 chondrite parent body requires more complicated mechanism for the moving and incorporating process of the clasts. For example, only upper layers of the clast parent body might be disrupted and mixed as breccias (i.e., large portions of CV3 chondrite formation layers and small portions of the clast formation layers were mixed). The breccia that is a chaotic mixture of CV3 chondrites, less-metamorphosed clasts, and metamorphosed clasts might exist, although such meteorite has not been found yet. Alternatively, the clasts might be derived from some selective phreatic emplacement, perhaps as a result of dehydration in the interior of the CV3 chondrite parent body (not onion shell model as Fig. 7), and mixed with CV3 chondrite materials (e.g., Kojima and Tomeoka 1996; Fu et al. 2017). Further studies are needed to constrain the clasts moving and incorporating process and thermal history of the CV3 chondrite parent body.

Comparison of the Accretion Age of the Clast Parent Body and the Formation Timing of CV3 Chondrules

If the clasts formed in the same parent body as the CV3 chondrites, the body should have accreted later than the formation timing of chondrules in CV3 chondrites. Note that the following discussion is based on the assumption that the clast parent body had an onion shell structure as Fig. 7.

The accretion ages of the clast parent body with 30–200 km radius and peak temperature of 800–1100 °C is 2.5–2.6 Ma to 2.1–2.2 Ma after CAI formation (Fig. 6). The errors on these calculated accretion ages are 0.1 Myr based on variations of the modeling parameters in the thermal modeling (see the Thermal Modeling of the CV3-Like Body section). Thus, the accretion age of the clast parent body including errors is 2.4–2.7 Ma to 2.0–2.3 Ma after CAI formation (black squares in Fig. 8). In contrast, the formation ages of chondrules in CV3 chondrites including errors are 2.1–2.5 Ma after CAI formation for Efremovka, 2.8–4.6 Ma after CAI formation for Vigarano, and 1.8–3.9 Ma after CAI formation for Kaba based on their initial $^{26}Al/^{27}Al$ ratios with 2σ errors (e.g., Mishra and Chaussidon 2014; Nagashima et al. 2017) (gray squares in Fig. 8).

The accretion ages of the clast parent body with peak temperature of 800–1100 °C is consistent with the formation ages of Efremovka and Kaba chondrules, but 0.1–0.5 Myr older than that of Vigarano chondrules (Fig. 8). These results suggest that the clasts and Efremovka and Kaba chondrites could be originated from the same parent body with peak temperature of 800–1100 °C that accreted immediately after the formation of Efremovka and Kaba chondrules. Vigarano might be derived from the different CV3 parent body, because the accretion age of the clast parent body becomes 0.1–0.5 Myr older than the

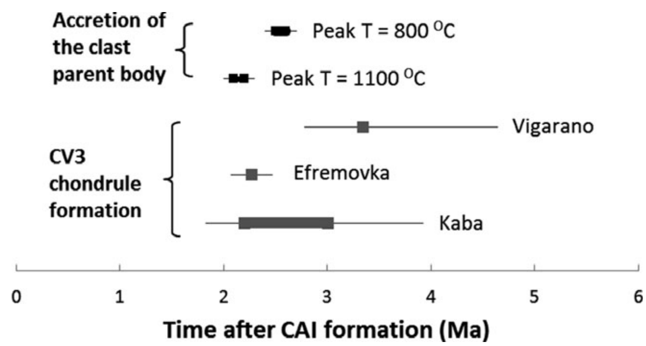

Fig. 8. Accretion age of the clast parent body (black square) and its comparison with formation age of chondrules in the CV3 Vigarano, Efremovka, and Kaba chondrites (gray square). The error on the accretion age of the clast parent body is ~0.1 Myr based on variations of the modeling parameters (see the Thermal Modeling of the CV3-Like Body section); the errors on the chondrule formation ages are estimated from 2σ errors of the initial $^{26}Al/^{27}Al$ ratios of chondrules (Mishra and Chaussidon 2014; Nagashima et al. 2017).

Vigarano chondrule formation age. If the clast parent body has a higher peak temperature than 1100 °C, the time difference between the accretion age of the body and the Vigarano chondrule formation age becomes large (>0.5 Myr) and the multiple CV3 parent model may become plausible.

SUMMARY

We observed 21 metamorphosed clasts in four CV3 chondrite breccias (GRA 06101, Vigarano, RBT 04143, and Y-86009). The observed clasts have similar mineralogical and petrological characteristics to those in the CV3 Mokoia and Y-86009 breccias (Jogo et al. 2012). We performed REE measurements on olivine, diopside, plagioclase, and spinel in the metamorphosed clasts 1–3 and 6 in the Y-86009 chondrite. Although the clasts in the CV3 Mokoia and Y-86009 breccias have similar oxygen isotopic compositions to CK chondrites and to a certain extent ureilites, we found that the REE compositions of the clasts in Y-86009 and these meteorites are different. This suggests that the clasts could not be fragments of these meteorites. REE compositions for each of the minerals in the clasts could reflect their precursor compositions (i.e., CV3 chondrites), or might be disturbed during thermal metamorphism in the CV3 chondrite parent body. Thermal modeling indicates that the CV3 chondrite parent body containing clasts would have accreted earlier than 2.5–2.6 Ma after CAI formation in order to reach the metamorphosed temperatures of the clasts of ≥800 °C. The clasts and CV3 chondrites could be originated from the same parent body with a peak temperature of 800–1100 °C. If the clast parent body has a higher peak temperature than 1100 °C, the accretion age of the body becomes older than the CV3 chondrule formation ages and the multiple CV3 parent model may become plausible.

Acknowledgments—The meteoritic samples of LAP 022066, LAP 04843, LAP 02228, MET 00430, MET 01074, QUE 97186, TIL 07007, A 881317, GRA 06101, RBT 04143, and Y-86009 were provided by Korea Polar Research Institute; National Institute of Polar Research, Japan; and NASA Johnson Space Center. The manuscript was improved by constructive comments from Prof. Tomoki Nakamura. Constructive reviews by Dr. P. C. Buchanan and R. Greenwood are highly appreciated. We thank Ms. Jung Jin Moon and Dr. Changkun Park for the support to use SEM and FE-EPMA at Korea Polar Research Institute. Thermal modeling was carried out on the PC cluster at the Center for Computational Astrophysics, National Astronomical Observatory of Japan. K. J. was supported by Korea Polar Research Institute project PE19230. M. I. was partly supported by the JSPS Grants-in-Aid for Science Research (no. 18K18795, 18H04468), and the Shimadzu Science Foundation (2016). This work was supported in part by the Kochi Core Center Open Facility System (KOFS) under the MEXT foundation. We have no conflict of interest to declare.

Editorial Handling—Dr. Michael Zolensky

REFERENCES

Anders E. and Grevesse N. 1989. Abundances of the elements: Meteoritic and solar. *Geochimica et Cosmochimica Acta* 53:197–214.

Ash R. D., Young E. D., Rumble III D., Alexander C. M. O'D., and MacPherson G. J. 1999. Oxygen isotope systematics in Allende chondrules (abstract #1836). 30th Lunar and Planetary Science Conference. CD-ROM.

Bischoff A., Palme H., Spettel B., Clayton R. N., and Mayeda T. K. 1988. The chemical composition of dark inclusions from the Allende meteorite (abstract). 19th Lunar and Planetary Science Conference. p. 88–89.

Bland P. A., Alard O., Benedix G. K., Kearsley A. T., Menzies O. N., Watt L. E., and Rogers N. W. 2005. Volatile fractionation in the early solar system and chondrule matrix complementarity. *Proceedings of the National Academy of Sciences* 39:13,755–13,760.

Bland P. A., Jackson M. D., Coker R. F., Cohen B. A., Webber J. B. W., Lee M. R., Duffy C. M., Chater R. J., Ardakani M. G., McPhail D. S., McComb D. W., and Benedix G. K. 2009. Why aqueous alteration in asteroids was isochemical: High porosity—high permeability. *Earth and Planetary Science Letters* 287:559–568.

Bonal L., Quirico E., Bourot-Denise M., and Montagnac G. 2006. Determination of the etrologic type of CV3 chondrites by Raman spectroscopy of included organic matter. *Geochimica et Cosmochimica Acta* 70:1849–1863.

Brearley A. J. 1997. Disordered biopyriboles, amphibole, and talc in the Allende meteorite: Products of nebular or parent body aqueous alteration? *Science* 276:1103–1105.

Brearley A. J. 1999. Origin of graphitic carbon and pentlandite in matrix olivines in the Allende meteorite. *Science* 285:1380–1382.

Brearley A. J. and Jones R. H. 1998. Chondritic meteorites. In *Planetary materials*, edited by Papike J. J. Reviews in Mineralogy, vol. 36. Washington, D.C.: Mineralogical Society of America. pp. 3-001–3-398.

Carporzen L., Weiss B. P., Elkins-Tanton L. T., Shuster D. L., Ebel D., and Gattacceca J. 2011. Magnetic evidence for a partially differentiated carbonaceous chondrite parent body. *Proceedings of the National Academy of Sciences* 108:6386–6389.

Chambers J. E. 2010. Planetesimal formation by turbulent concentration. *Icarus* 208:505–517.

Chaumard N. and Devouard B. 2016. Chondrules in CK carbonaceous chondrites and thermal history of the CV–CK parent body. *Meteoritics & Planetary Science* 51:547–573.

Chaumard N., Devouard B., Bouvier A., and Wadhwa M. 2014. Metamorphosed calcium-aluminum-rich inclusions in CK carbonaceous chondrites. *Meteoritics & Planetary Science* 49:419–452.

Cherniak D. J. 2010. REE diffusion in olivine. *American Mineralogist* 95:362–368.

Choi B. G., Krot A. N., and Wasson J. T. 2000. Oxygen isotopes in magnetite and fayalite in CV chondrites Kaba and Mokoia. *Meteoritics & Planetary Science* 35:1239–1248.

Clayton R. N. and Mayeda T. K. 1999. Oxygen isotope studies of carbonaceous chondrites. *Geochimica et Cosmochimica Acta* 63:2089–2104.

Clayton R. N., Mayeda T. K., Onuma N., and Shearer J. 1976. Oxygen isotopic composition of minerals in the Kenna ureilite. *Geochimica et Cosmochimica Acta* 40:1475–1476.

Cohen R. E., Kornacki A. S., and Wood J. A. 1983. Mineralogy and petrology of chondrules and inclusions in the Mokoia CV3 chondrite. *Geochimica et Cosmochimica Acta* 47:1739–1757.

Connelly J. N., Bizzarro M., Krot A. N., Nordlund A., Wielandt D., and Ivanova M. A. 2012. The absolute chronology and thermal processing of solids in the solar protoplanetary disk. *Science* 338:651–655.

Consolmagno G., Britt D., and Macke R. 2008. The significance of meteorite density and porosity. *Chemie der Erde* 68:1–29.

Cosarinsky M., Leshin L. A., MacPherson G. J., Guan Y., and Krot A. N. 2008. Chemical and oxygen isotopic compositions of accretionary rim and matrix olivine in CV chondrites: Constraints on the evolution of nebular dust. *Geochimica et Cosmochimica Acta* 72:1887–1913.

Curtis D. B. and Schmitt R. A. 1979. The petrogenesis of L-6 chondrites: Insights from the chemistry of minerals. *Geochimica et Cosmochimica Acta* 43:1091–1103.

Cuzzi J. N., Hogan R. C., and Shariff K. 2008. Toward planetesimals: Dense chondrule clumps in the protoplanetary nebula. *The Astrophysical Journal* 687:1432–1447.

Dohmen R. and Chakraborty S. 2007. Fe–Mg diffusion in olivine II: Point defect chemistry, change of diffusion mechanisms and a model for calculation of diffusion coefficients in natural olivine. *Physics and Chemistry of Minerals* 34:409–430.

Doyle P. M., Jogo K., Nagashima K., Krot A. N., Wakita S., Ciesla F., and Hutcheon I. 2015. Early aqueous activity on the ordinary and carbonaceous chondrite parent asteroids recorded by fayalite. *Nature Communications* 6:7444.

Elkins-Tanton L. T., Weiss B. P., and Zuber M. T. 2011. Chondrites as samples of differentiated planetesimals. *Earth and Planetary Science Letters* 305:1–10.

Fabries J. 1979. Spinel-olivine geothermometry in peridotites from ultramafie complexes. *Contributions to Mineralogy and Petrology* 69:329–336.

Fahey A. J. 1998. Details of the measurement of rare earth and other trace element abundances by secondary ion mass spectrometry. *International Journal of Mass Spectrometry* 176:63–76.

Floss C. 2000. Complexities on the acapulcoite-lodranite parent body: Evidence from trace element distributions in silicate minerals. *Meteoritics & Planetary Science* 35:1073–1085.

Fruland R. M., King E. A., and McKay D. S. 1978. Allende dark inclusions. Proceedings, 9th Lunar and Planetary Science Conference. pp. 1305–1329.

Fu R. R. and Elkins-Tanton L. T. 2014. The fate of magmas in planetesimals and the retention of primitive chondritic crusts. *Earth and Planetary Science Letters* 390:128–137.

Fu R. R., Young E. D., Greenwood R. C., and Elkins-Tanton L. T. 2017. Silicate melting and volatile loss during differentiation in planetesimals. In *Planetesimals: Early differentiation and consequences for planets*, edited by Elkins-Tanton L. and Weiss B. Cambridge, UK: Cambridge University Press. pp. 115–135.

Ganino C. and Libourel G. 2017. Reduced and unstratified crust in CV chondrite parent body. *Nature Communications* 8:261.

Greenwood R. C., Franchi I. A., Kearsley A. T., and Alard O. 2010. The relationship between CK and CV chondrites. *Geochimica et Cosmochimica Acta* 74:1684–1705.

Grove T. L., Baker M. B., and Kinzler R. J. 1984. Coupled CaAl-NaSi diffusion in plagioclase feldspar: Experiments and applications to cooling rate speedometry. *Geochimica et Cosmochimica Acta* 48:2113–2121.

Guan Y. and Crozaz G. 2000. Light rare earth element enrichments in ureilites: A detailed ion microprobe study. *Meteoritics & Planetary Science* 35:131–144.

Holland T. J. B. and Powell R. 1998. An internally consistent thermodynamic data set for phases of petrological interest. *Journal of Metamorphic Geology* 16:309–343.

Hua X., Zinner E. K., and Buseck P. R. 1996. Petrography and chemistry of fine-grained dark rims in the Mokoia CV3 chondrite: Evidence for an accretionary origin. *Geochimica et Cosmochimica Acta* 60:4265–4274.

Hua X., Huss G. R., Tachibana S., and Sharp T. G. 2005. Oxygen, silicon, and Mn-Cr isotopes of fayalite in the Kaba oxidized CV3 chondrite: Constraints for its formation history. *Geochimica et Cosmochimica Acta* 69:1333–1348.

Hutchison R. 2007. *Meteorites: A petrologic, chemical and isotopic synthesis*. Cambridge, UK: Cambridge University Press.

Ikeda Y. and Kimura M. 1995. Anhydrous alteration of Allende chondrules in the solar nebula I Description and alteration of chondrules with known oxygen-isotopic components. *Proceedings of the NIPR Symposium on Antarctic Meteorites* 8:97–122.

Inoue M., Kimura M., and Nakamura N. 2004. REE abundances in the matrix of the Allende (CV) meteorite: Implications for matrix origin. *Meteoritics & Planetary Science* 39:599–608.

Irving A. J., Larson T. E., Longstaffe F. J., Rumble D., Bunch T. E., Wittke J. H., and Kuehner S. M. 2004. A primitive achondrite with oxygen isotopic affinities to CV chondrites: Implications for differentiation and size of the CV parent body (abstract). American Geophysical Union. P31C–02.

Ito M. and Messenger S. 2016. Rare earth element measurements and mapping of minerals in the Allende CAI, 7R19-1, by NanoSIMS ion microprobe. *Meteoritics & Planetary Science* 51:818–832.

Jabeen I., Kusakabe M., Nakamura T., and Nagao K. 1998. Oxygen isotopic signature in Allende chondrules (abstract). *Meteoritics & Planetary Science* 33:A76–A77.

Jabeen I., Kusakabe M., Nakamura T., and Nagao K. 1999. Parent body processes in Allende: Evidence from oxygen isotope study of the Allende chondrules (abstract). *Proceedings of the NIPR Symposium on Antarctic Meteorites* 24:59–61.

Jacquet E., Alard O., and Gounelle M. 2012. Chondrule trace element geochemistry at the mineral scale. *Meteoritics & Planetary Science* 47:1695–1714.

Jogo K., Nakamura T., Noguchi T., and Zolotov M. Y. 2009. Fayalite in the Vigarano CV3 carbonaceous chondrite: Occurrences, formation age and conditions. *Earth and Planetary Science Letters* 287:320–328.

Jogo K., Nagashima K., Hutcheon I. D., Krot A. N., and Nakamura T. 2012. Heavily metamorphosed clasts from the CV chondrite breccias Mokoia and Yamato-86009. *Meteoritics & Planetary Science* 47:2251–2268.

Jogo K., Nakamura T., Ito M., Wakita S., Zolotov M. Y., and Messenger S. R. 2017. Mn–Cr ages and formation conditions of fayalite in CV3 carbonaceous chondrites: Constraints on the accretion ages of chondritic asteroids. *Geochimica et Cosmochimica Acta* 199:58–74.

Jogo K., Ito M., Nakamura T., Kobayashi S., and Lee J. 2018. Redistribution of Sr and rare earth elements in the matrices of CV3 carbonaceous chondrites during aqueous alteration in their parent body. *Earth, Planets and Space* 70:37.

Johansen A., Oishi J. S., Mac Low M., Klahr H., Henning T., and Youdin A. 2007. Rapid planetesimal formation in turbulent circumstellar disks. *Nature* 448:1022–1025.

Johnson C. A., Prinz M., Weisberg M. K., Clayton R. N., and Mayeda T. K. 1990. Dark inclusions in Allende, Leoville, and Vigarano: Evidence for nebular oxidation of CV3 constituents. *Geochimica et Cosmochimica Acta* 54:819–830.

Jurewicz A. J. G., Mittlefieldt D. W., and Jones J. H. 1993. Experimental partial melting of the Allende (CV) and Murchison (CM) chondrites and the origin of asteroidal basalts. *Geochimica et Cosmochimica Acta* 57:2123–2139.

Keller L. P., Thomas K. L., Clayton R. N., Mayeda T. K., DeHart J. M., and McKay D. S. 1994. Aqueous alteration of the Bali CV3 chondrite: Evidence from mineralogy, mineral chemistry, and oxygen isotopic compositions. *Geochimica et Cosmochimica Acta* 58:5589–5598.

Kimura M. and Ikeda Y. 1995. Anhydrous alteration of Allende chondrules in the solar nebula II: Alkali-Ca exchange reactions and formation of nepheline, sodalite and Ca-rich phases in chondrules. *Proceedings of the NIPR Symposium on Antarctic Meteorites* 8:123–138.

Kita N. T., Yin Q., MacPherson G. J., Ushikubo T., Jacobsen B., Nagashima K., Kurahashi E., Krot A. N., and Jacobsen S. B. 2012. ^{26}Al-^{26}Mg isotope systematics of the first solids in the early solar system. *Meteoritics & Planetary Science* 48:1383–1400.

Kojima T. and Tomeoka K. 1996. Indicators of aqueous alteration and thermal metamorphism on the CV parent body: Microtextures of a dark inclusion from Allende. *Geochimica et Cosmochimica Acta* 60:2651–2666.

Kracher A., Keil K., Kallemeyn G. W., Wasson J. T., Clayton R. N., and Huss G. I. 1985. The Leoville (CV3) accretionary breccia. *Journal of Geophysical Research—Solid Earth* 90:123–135.

Kretz R. 1982. Transfer and exchange equilibria in a portion of the pyroxene quadrilateral as deduced from natural and experimental data. *Geochimica et Cosmochimica Acta* 46:411–421.

Krot A. N. and Hutcheon I. D. 1997. Highly oxidized and metamorphosed chondritic or igneous (?) clasts in the CV3 carbonaceous chondrite Mokoia: Excavated material from the interior of the CV3 asteroid or previously unsampled asteroid (abstract #1347). 28th Lunar and Planetary Science Conference. CD-ROM.

Krot A. N., Scott E. R. D., and Zolensky M. E. 1995. Mineralogical and chemical modification of components in CV3 chondrites: Nebular or asteroidal processing? *Meteoritics* 30:748–775.

Krot A. N., Petaev M. I., Scott E. R. D., Choi B., Zolensky M. E., and Keil K. 1998a. Progressive alteration in CV3 chondrites: More evidence for asteroidal alteration. *Meteoritics & Planetary Science* 33:1065–1085.

Krot A. N., Zolensky M. E., Keil K., Scott E. R. D., and Nakamura K. 1998b. Secondary Ca-Fe-rich minerals in the Bali-like and Allende-like oxidized CV3 chondrites and Allende dark inclusions. *Meteoritics & Planetary Science* 33:623–645.

Krot A. N., Meibom A., and Keil K. 2000a. A clast of Bali-like oxidized CV material in the reduced CV chondrite breccia Vigarano. *Meteoritics & Planetary Science* 35:817–825.

Krot A. N., Petaev M. I., Meibom A., and Keil K. 2000b. In situ growth of Ca-rich rims around Allende dark inclusions. *Geochemistry International* 38:351–368.

Krot A. N., Petaev I. M., and Bland P. A. 2004. Multiple formation mechanisms of ferrous olivine in CV carbonaceous chondrites during fluid-assisted metamorphism. *Antarctic Meteorite Research* 17:153–171.

Krot A., Yurimoto H., McKeegan K., Leshin L., Chaussidon M., Libourel G., Yoshitake M., Huss G., Guan Y., and Zanda B. 2006. Oxygen isotopic compositions of chondrules: Implications for evolution of oxygen isotopic reservoirs in the inner solar nebula. *Chemie der Erde—Geochemistry* 66:249–276.

Lodders K. 2003. Solar system abundances and condensation temperatures of the elements. *The Astrophysical Journal* 591:1220–1247.

MacPherson G. J. and Krot A. N. 2014. The formation of Ca-, Fe-rich silicates in reduced and oxidized CV chondrites: The roles of impact-modified porosity and permeability, and heterogeneous distribution of water ices. *Meteoritics & Planetary Science* 49:1250–1270.

MacPherson G. J., Davis A. M., and Zinner E. K. 1995. The distribution of aluminum-26 in the early solar system—A reappraisal. *Meteoritics* 30:365–386.

MacPherson G. J., Nagashima K., Krot A. N., Doyle P. M., and Ivanova M. 2017. ^{53}Mn–^{53}Cr chronology of Ca–Fe silicates in CV3 chondrites. *Geochimica et Cosmochimica Acta* 201:260–274.

Martin C., Debaille V., Lanari P., Goderis S., Vandendael I., Vanhaecke F., Vidal O., and Claeys P. 2013. REE and Hf distribution among mineral phases in the CV–CK clan: A way to explain present-day Hf isotopic variations in chondrites. *Geochimica et Cosmochimica Acta* 120:496–513.

McSween H. Y. Jr. 1977. Petrographic variations among carbonaceous chondrites of the Vigarano type. *Geochimica et Cosmochimica Acta* 41:1777–1790.

Mishra R. K. and Chaussidon M. 2014. Timing and extent of Mg and Al isotopic homogenization in the early inner Solar System. *Earth and Planetary Science Letters* 390:318–326.

Nagashima K., Krot A. N., and Komatsu M. 2017. ^{26}Al–^{26}Mg systematics in chondrules from Kaba and Yamato 980145 CV3 carbonaceous chondrites. *Geochimica et Cosmochimica Acta* 201:303–319.

Righter K. and Neff K. E. 2007. Temperature and oxygen fugacity constraints on CK and R chondrites and implications for water and oxidation in the early solar system. *Polar Science* 1:25–44.

Rubin A. E. 1993. Dikes vs. diapirs in viscoelastic rock. *Earth and Planetary Science Letters* 117:653–670.

Schoenbeck T. W., Kleine T., and Irving A. J. 2006. Chemical and Hf-W isotopic composition of CV metachondrite NWA 3133 (abstract #1550). 37th Lunar and Planetary Science Conference. CD-ROM.

Shah J., Bates H. C., Muxworthy A. R., Hezel D. C., Russell S. S., and Gengea M. J. 2017. Long-lived magnetism on chondrite parent bodies. *Earth and Planetary Science Letters* 475:106–118.

Spivak-Brindorf L. J., Wadhwa M., and Janney P. E. 2011. ^{60}Fe-^{60}Ni chronology of the D'Orbigny angrite: Implications for the initial solar system abundance of ^{60}Fe (abstract #2281). 42nd Lunar and Planetary Science Conference. CD-ROM.

Stracke A., Palme H., Gellissen M., Münker C., Kleine T., Birbaum K., Günther D., Bourdon B., and Zipfel J. 2012. Refractory element fractionation in the Allende meteorite: Implications for solar nebula condensation and the chondritic composition of planetary bodies. *Geochimica et Cosmochimica Acta* 85:114–141.

Tang H. and Dauphas N. 2011. Constraints from achondrites on the initial ^{60}Fe/^{56}Fe ratio of the solar system (abstract #1068). 42nd Lunar and Planetary Science Conference. CD-ROM.

Telus M., Huss G. R., Nagashima K., Ogliore R. C., Tachibana S., and Jilly C. E. 2011. Possible heterogeneity of ^{60}Fe in chondrules from primitive ordinary chondrites (abstract #2559). 42nd Lunar and Planetary Science Conference. CD-ROM.

Telus M., Huss G. R., Ogliore R. C., Nagashim K., Howard D. L., Newville M. G., and Tomkins A. G. 2016. Mobility of iron and nickel at low temperatures: Implications for ^{60}Fe–^{60}Ni systematics of chondrules from unequilibrated ordinary chondrites. *Geochimica et Cosmochimica Acta* 178:87–105.

Tomeoka K. and Tanimura I. 2000. Phyllosilicate-rich chondrule rims in the Vigarano CV3 chondrite: Evidence for parent-body processes. *Geochimica et Cosmochimica Acta* 64:1971–1988.

Wakita S. and Sekiya M. 2011. Thermal evolution of icy planetesimals in the solar nebula. *Earth, Planets and Space* 63:1193–1206.

Wasserburg G. J., Hutcheon I. D., Aléon J., Ramon E. C., Krot A. N., Nagashima K., and Brearley A. J. 2011. Extremely Na- and Cl-rich chondrule from the CV3 carbonaceous chondrite Allende. *Geochimica et Cosmochimica Acta* 75:4752–4770.

Wasson J. T., Isa J., and Rubin A. E. 2013. Compositional and petrographic similarities of CV and CK chondrites: A single group with variations in textures and volatile concentrations attributable to impact heating, crushing and oxidation. *Geochimica et Cosmochimica Acta* 108:45–62.

Weisberg M. K., Printz M., Clayton R., and Mayeda T. K. 1997. CV3 chondrites: Three subgroups, not two (abstract). *Meteoritics & Planetary Science* 32:138–139.

Wilson L., Keil K., Browning L. B., Krot A. N., and Bourcier W. 1999. Early aqueous alteration, explosive disruption, and reprocessing of asteroids. *Meteoritics & Planetary Science* 34:541–557.

Young E. D., Ash R. D., England P., and Rumble D. 1999. Fluid flow in chondritic parent bodies: Deciphering the compositions of planetesimals. *Science* 286:1331–1335.

Zolotov M. Y., Mironenko M. V., and Shock E. L. 2006. Thermodynamic constraints on fayalite formation on parent bodies of chondrites. *Meteoritics & Planetary Science* 41:1775–1796.

SUPPORTING INFORMATION

Additional supporting information may be found in the online version of this article:

Table S1. Relative sensitivity factors and monoxide ion production ratios in standards.

Table S2. Representative electron microprobe analyses (in wt%) of the major minerals in metamorphosed clasts in GRA 06101, Vigarano, RBT 04143, and Y 86009.

Table S3. REE concentrations (ppb) in various phases of the metamorphosed clasts 1, 2, 3 and 6 in the Y 86009 chondrite.

Fig. S1. Comparison of diffusion coefficients of Fe-Mg (blue line: Dohmen and Chakraborty 2007) in olivine, REEs in olivine (red line: Cherniak 2010) and CaAl-NaSi in plagioclase (green line: Grove et al. 1984) under fO_2 of CV3 chondrites.